

● *Original Contribution for the Festschrift in honor of Robert C. Waag*

## MOUSE LIVER DISPERSION FOR THE DIAGNOSIS OF EARLY-STAGE FATTY LIVER DISEASE: A 70-SAMPLE STUDY

CHRISTOPHER T. BARRY,\* ZAEGYOO HAH,<sup>†</sup> ALEXANDER PARTIN,<sup>†</sup> ROBERT A. MOONEY,<sup>‡</sup>  
KUANG-HSIANG CHUANG,\* ALICIA AUGUSTINE,<sup>§</sup> ANTHONY ALMUDEVAR,<sup>||</sup> WENQING CAO,<sup>‡</sup>  
DEBORAH J. RUBENS,<sup>||,¶</sup> and KEVIN J. PARKER<sup>†</sup>

\*Department of Surgery, University of Rochester Medical Center, Rochester, New York, USA; <sup>†</sup>Department of Electrical & Computer Engineering, University of Rochester, Rochester, New York, USA; <sup>‡</sup>Department of Pathology and Laboratory Medicine, University of Rochester Medical Center, Rochester, New York, USA; <sup>§</sup>Department of Public Health Services, University of Rochester Medical Center, Rochester, New York, USA; <sup>||</sup>Department of Biostatistics and Computational Biology, University of Rochester Medical Center, Rochester, New York, USA; and <sup>¶</sup>Department of Radiology, University of Rochester Medical Center, Rochester, New York, USA

(Received 27 June 2013; revised 15 October 2013; in final form 21 October 2013)

**Abstract**—The accumulation of fat droplets within the liver is an important marker of liver disease. This study assesses gradations of steatosis in mouse livers using crawling waves, which are interfering patterns of shear waves introduced into the liver by external sources. The crawling waves are detected by Doppler ultrasound imaging techniques, and these are analyzed to estimate the shear wave speed as a function of frequency between 200 and 360 Hz. In a study of 70 mice with progressive increases in steatosis from 0% to >60%, increases in steatosis are found to increase the dispersion, or frequency dependence, of shear wave speed. This finding confirms an earlier, smaller study and points to the potential of a scoring system for steatosis based on shear wave dispersion. (E-mail: [kevin.parker@rochester.edu](mailto:kevin.parker@rochester.edu)) © 2014 World Federation for Ultrasound in Medicine & Biology.

**Key Words:** Fatty liver disease, Steatosis, Dispersion, Crawling waves, Shear wave elasticity imaging, Medical ultrasound imaging, Viscoelastic tissue models.

### INTRODUCTION

As a result of the unabated obesity epidemic, fatty liver disease (FLD) is the most common cause of liver dysfunction in the United States and other economically privileged countries (Angulo 2002; Dowman et al. 2010; Schreuder et al. 2008). Accumulation of fat droplets (steatosis) within the liver is most often associated with the metabolic syndrome of obesity, diabetes and dyslipidemia, but can also be caused by toxins such as alcohol and certain chemotherapeutic agents or, rarely, associated with pregnancy (Charlton 2004; Marchesini et al. 1999; Wanless and Lentz 1990). Simple hepatic steatosis is reversible, but can progress to a chronic inflammatory and fibrotic state termed NASH (non-alcoholic steatohepatitis). Cirrhosis caused by NASH is predicted to become the leading cause of end-stage

liver failure and indication for liver transplant in this country within the next 8 y (Charlton 2004; Selzner and Clavien 2001).

Liver biopsy currently remains the gold standard for diagnosing and assessing FLD (Minervini et al. 2009). Because this procedure is uncomfortable and can rarely result in serious complications, the current practice is to reserve biopsy for patients in whom the suspicion for NASH is high (based on blood testing or imaging) (Strassburg and Manns 2006). Unfortunately, biochemical assessment and currently available imaging modalities are insensitive in determining the presence or degree of FLD. Furthermore, histologic assessment of liver biopsies is completely subjective (based on the individual pathologist's estimation of overall steatosis and fibrosis) and, therefore, subject to wide clinical variability.

Non-invasive techniques to assess hepatic steatosis are emerging to meet this critical need and include magnetic resonance elastography (Chen et al. 2011; Salameh et al. 2009; Schwenzer et al. 2009), magnetic resonance

Address correspondence to: Kevin J. Parker, University of Rochester, Hopeman Building 203, PO Box 270126, Rochester, NY 14627-0126, USA. E-mail: [kevin.parker@rochester.edu](mailto:kevin.parker@rochester.edu)

spectroscopy (Friedrich-Rust *et al.* 2010), computed tomography elastography (Castera *et al.* 2008), radiation force methods (Chen *et al.* 2013) and controlled attenuation parameter transient elastography (de Ledinghen *et al.* 2012; Friedrich-Rust *et al.* 2012; Sasso *et al.* 2010, 2012). We propose an ultrasound-based system that can serve as a point of care screening modality (*i.e.*, available to primary care physicians and gastroenterologists) to complement and increase efficient use of biopsy and other more costly imaging techniques.

Our previous work (Barry *et al.* 2012) introduced the hypothesis that increasing the amount of fat in the liver would increase the dispersion of shear wave velocity, resulting in an increase in the slope of shear speed and shear attenuation versus frequency. This is a consequence of adding a viscous element, triglycerides, to the liver medium. This previous study reported results from a preliminary study of 14 mice divided into two groups, lean (<5% steatosis) and obese (~65% steatosis). The difference in dispersion or slope of shear speed versus frequency between the two groups was found to be statistically significant ( $p < 0.003$ ) Dispersion was low in lean livers ( $0.16 \pm 0.03$  m/s per 100 Hz) and higher in obese livers ( $0.23 \pm 0.04$  m/s per 100 Hz), as measured over a shear wave frequency band centered around 260 Hz.

In the present study, we expand the numbers of mice and attempt to titrate the response by examining subgroups with increasing steatosis. Ultimately the goal is to establish a fine gradation scoring of steatosis using shear wave dispersion, *in vivo*. The present study takes a first step toward that goal.

## THEORY

### Shear wave dispersion

To model shear wave propagation in sinusoidal steady state in an elastic material with losses, the general stress-strain relationship is

$$T(\omega) = \mu S(\omega) \quad (1)$$

where  $T$  and  $S$  are the shear stress and strain, respectively,  $\omega$  is the frequency and  $\mu$  is the shear modulus; the shear wave speed  $c_s = \sqrt{\mu/\rho}$ , where  $\rho$  is density. Assuming that  $\mu$  can be described as  $\mu(\omega) = K(\omega) + jH(\omega)$ , where  $K$  is the real part and  $H$  is the imaginary part of the shear modulus, then the complex wavenumber is

$$k = \frac{\omega}{c_s} = \beta - j\alpha = \frac{\omega}{\sqrt{\frac{K(\omega) + jH(\omega)}{\rho}}} \quad (2)$$

Here,  $k$  is the wavenumber with real ( $\beta$ ) and imaginary ( $\alpha$ ) parts (Blackstock 2000). The attenuation coefficient,  $\alpha$ , of a propagating wave will therefore be a function of

frequency depending on  $K(\omega)$  and  $H(\omega)$ . Expanding on the real and imaginary parts of eqn (2), we have

$$\beta = \omega \sqrt{\frac{\rho}{K^2 + H^2}} \left[ \frac{1}{2} \left( 1 + \frac{1}{\sqrt{1 + \frac{H^2}{K^2}}} \right) \right]^{\frac{1}{2}} \quad (3)$$

and the wave speed

$$c = \sqrt{\frac{\sqrt{K^2 + H^2}}{\rho}} \left[ \frac{1}{2} \left( 1 + \frac{1}{\sqrt{1 + \frac{H^2}{K^2}}} \right) \right]^{-\frac{1}{2}} \quad (4)$$

and the absorption coefficient

$$\begin{aligned} \alpha &= \omega \sqrt{\frac{\rho}{\sqrt{K^2 + H^2}}} \left[ \frac{1}{2} \left( 1 - \frac{1}{\sqrt{1 + \frac{H^2}{K^2}}} \right) \right]^{\frac{1}{2}} \\ &= \frac{\omega}{c} \sqrt{\frac{1 - \frac{1}{\sqrt{1 + \frac{H^2}{K^2}}}}{1 + \frac{1}{\sqrt{1 + \frac{H^2}{K^2}}}}} \end{aligned} \quad (5)$$

Note that if  $H(\omega)$  is zero, then  $c$  and  $\beta$  are constant (over frequency), and  $\alpha$  is zero. However, if  $H(\omega)$  is non-zero, then  $c$  and  $\alpha$  have a slope versus frequency and are termed “dispersive.” From these relations, dispersion measurements are found to indicate the presence of a loss term in the material properties.

### Crawling waves

The crawling wave technique, introduced by Wu *et al.* (2004), is an elasticity imaging method used to map elastic properties within biomaterials. It is a slowly propagating pattern of interfering shear waves, generated in the medium *via* non-invasive sources. Crawling wave (CrW) propagation can be implemented using external mechanical vibrations (Hoyt *et al.* 2008b; Partin *et al.* *in press*; Wu *et al.* 2006) as well as acoustic radiation force (Hah *et al.* 2012; Hazard *et al.* 2012). CrW data acquired by an ultrasound system can be further analyzed to estimate shear parameters (shear speed or shear modulus) within the region of interest (ROI) and, thereby, used to quantify the elasticity of the scanned medium.

In this study, mechanical vibration sources are placed at opposite sides of a phantom to induce plane shear waves into a ROI using continuous harmonic vibrations, as illustrated in Figure 1. The sources are driven by sinusoidal signals with a slight difference between the frequencies  $f_1$  and  $f_2$ , such that  $(f_2 - f_1) \ll f$ . Subscripts 1 and 2 correspond to the left and right sources,

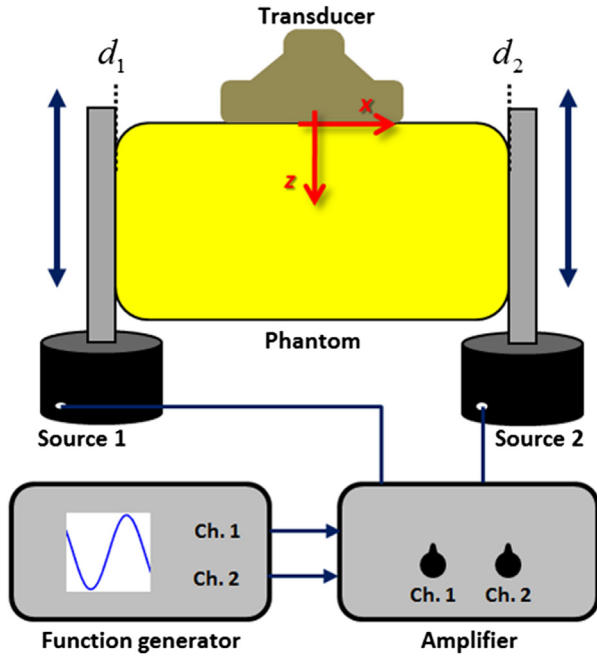


Fig. 1. Crawling wave experimental setup. A dual-channel function generator produces two sinusoidal signals with a slight difference of 0.6 Hz between the frequencies. The signals are amplified and supplied to piston vibration sources. The elongated bars mounted on the pistons vibrate along the  $z$ -axis and generate crawling wave propagation within the phantom. A linear array ultrasound transducer is positioned between the vibration sources and scans the medium.

respectively. The plane shear waves, propagating along the lateral direction ( $x$ -axis), are represented by

$$u_1(x, t) = A_1 e^{-\alpha_s(x-d_1)} e^{i[\omega_1 t - k_1(x-d_1) + \phi_1]} \quad (6)$$

and

$$u_2(x, t) = A_2 e^{-\alpha_s(d_2-x)} e^{i[\omega_2 t + k_2(x-d_2) + \phi_2]}, \quad (7)$$

where  $A$  is the vibration amplitude,  $\alpha_s$  is the attenuation coefficient for shear waves,  $d$  is the lateral location of the vibration source,  $\omega$  is the angular frequency of the shear wave ( $\omega = 2\pi f$ , where  $f$  is the vibration frequency),

$$\begin{aligned} |u_T(x, t)|^2 &= (u_1 + u_2) \cdot (u_1 + u_2)^* \\ &= A_1^2 e^{-2\alpha_s(x-d_1)} + A_2^2 e^{-2\alpha_s(d_2-x)} + 2A_1 A_2 \cos[(\omega_1 - \omega_2)t - (k_1 + k_2)x + k_1 d_1 + k_2 d_2 + \phi_1 - \phi_2] \\ &= B(x) + 2A_1 A_2 \cos(\Delta\omega t - 2kx + \phi) \end{aligned} \quad (9)$$

$k$  is the shear wavenumber and  $\phi$  is an arbitrary phase term. The shear waves are superimposed, and a moving interference pattern is created that is displayed in Doppler mode as “crawling” parallel stripes.

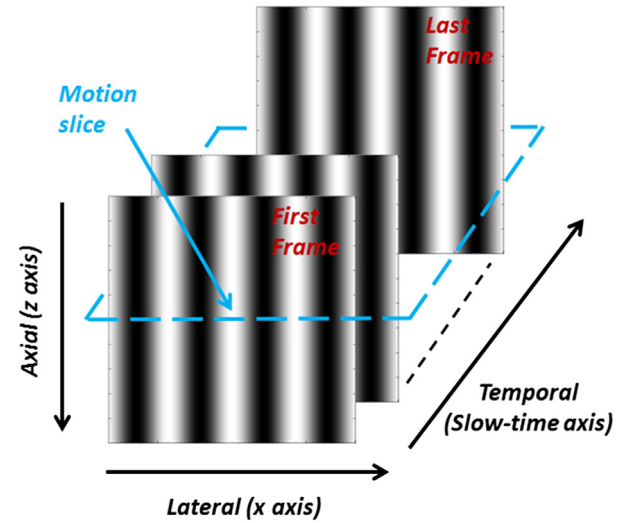


Fig. 2. Three-dimensional crawling wave data. The axial, lateral and slow-time axes correspond to the depth, width and time of the crawling wave movie, respectively. The motion slice, from which the shear speed is estimated, is outlined by the dashed line.

A 3-D matrix of power spectrum variance (axial  $\times$  lateral  $\times$  temporal), illustrated in Figure 2, is computed from the acquired Doppler data using an equation derived by Kasai et al. (1985):

$$\sigma^2 = \frac{2}{T_{\text{PRF}}} \left( 1 - \frac{|R(T_{\text{PRF}})|}{R(0)} \right), \quad (8)$$

Here  $T_{\text{PRF}}$  is the time interval between the successive ultrasound Doppler pulses, and  $R$  is the autocorrelation of the backscattered signals of a given Doppler packet. The Doppler imaging is employed with the following parameters:  $f_{\text{Doppler}} = 10$  MHz,  $\text{PRF} = 1/T_{\text{PRF}} = 1.3$  kHz and a Doppler packet of 16 echoes. The size of the 3-D spectrum variance matrix is on the order of  $7 \text{ mm} \times 4 \text{ mm} \times 10 \text{ s}$ . The variance of the Doppler power spectrum is proportional to the square amplitude of the particle displacements. By use of eqns (6) and (7), the displacement square of the interfering shear waves is

where  $B(x)$  is a baseline term,  $\omega_1 - \omega_2 = \Delta\omega$ ,  $k_1 \approx k_2 \approx k$  (as  $\Delta k = \Delta\omega/c_s \ll k$ ) and  $k_1 d_1 + k_2 d_2 + \phi_1 - \phi_2 = \phi$ .

Several approaches that estimate local shear speed have been developed and applied in previous studies

(Hoyt *et al.* 2007, 2008a; Partin *et al.* in press; Wu *et al.* 2004). Here, however, we assume that the medium is macroscopically homogeneous because liver steatosis and liver fibrosis are characterized by gross overall changes in liver viscoelastic properties.

Each vertical stripe of the CrW pattern corresponds to a set of data points of constant phase. A motion slice image, outlined in Figure 2, is extracted from the 3-D CrW data. The CrW stripes are displayed as diagonal lines in the motion slice, as illustrated in Figure 3. The diagonal lines represent data points of constant phase over the temporal-lateral plane. The average shear speed  $c_s$  within the scanned ROI is calculated as

$$c_s = 2 \frac{\omega}{\Delta\omega} \cdot \frac{dx}{dt}, \quad (10)$$

where  $dx$  and  $dt$  are extracted from the motion slice. Equation (10) was derived by differentiating the phase term of eqn (9),  $\Delta\omega t - 2kx + \phi$ , with respect to  $t$  as follows:

$$\Delta\omega \cdot dt - \frac{4\pi f}{c_s} \cdot dx = 0. \quad (11)$$

### METHODS

Seventy C57BL/6J mice purchased from Jackson Laboratories were housed in a micro-isolator room on a 12-h light/dark cycle at the University of Rochester. The University Committee on Animal Resources approved all protocols. At the age of 5 wk, the normal chow diet was switched to a high-fat diet (16.6% kcal/g protein, 59.3% kcal/g fat, 24.48% kcal/g carbohydrate) (No. S3282, Bioserve, Frenchtown, NJ, USA). The latter resulted in diet-induced obesity. Seventy mice were

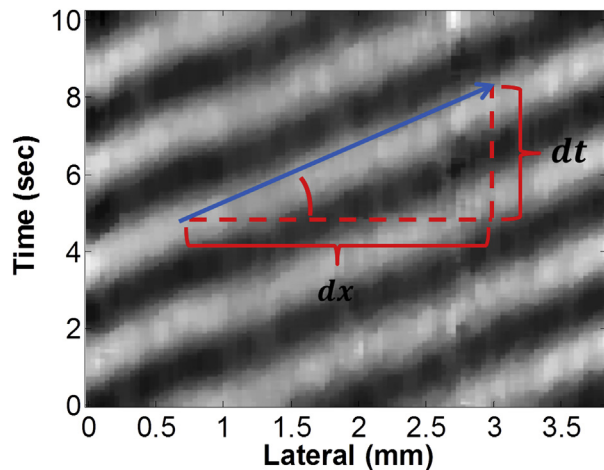


Fig. 3. A motion slice extracted from crawling wave data. The angle is indicative of the shear wave speed of the medium.

sacrificed for hepatectomy (surgical resection of the liver) 0, 4, 8, 11, 12, 13, 14, 15, 20 and 25 wk after being fed the high-fat diet. Whole-liver weights were in the range of approximately 10–20 g. This corresponds roughly to volumes of 10–20 mL.

After hepatectomy, two small portions of the liver were evaluated histologically and biochemically. Histologic examination of percentage hepatic steatosis was performed by a single, experienced pathologist (W.Q.C.) using hematoxylin and eosin-stained tissue sections (Klain *et al.* 1989). Triglyceride (TG, a representative of fat concentration [Levene *et al.* 2012]) assay was performed, and the results were reported as milligrams of TG per milligram of liver. The rest of the liver was suspended in a gelatin phantom for CrW scanning. The overall procedure executed for each liver sample is summarized in Figure 4.

The TG extraction protocol was modified from Burant *et al.* (1997). We weighed the frozen liver pieces and homogenized them in chloroform:methanol (2:1 v/v). Then we filtered extracts through fluted filter paper. Sulfuric acid (0.05% in saline) was added to filtered extract at a ratio of 1:5 (v/v). After centrifugation, the chloroform layer was removed, dried down and resuspended in fresh chloroform. Samples were then diluted in 5% Triton X-100 (Sigma) (in chloroform) and evaporated. Finally, we measured TG in duplicate using the L-Type Triglyceride Kit (Wako Chemicals, Richmond, VA, USA).

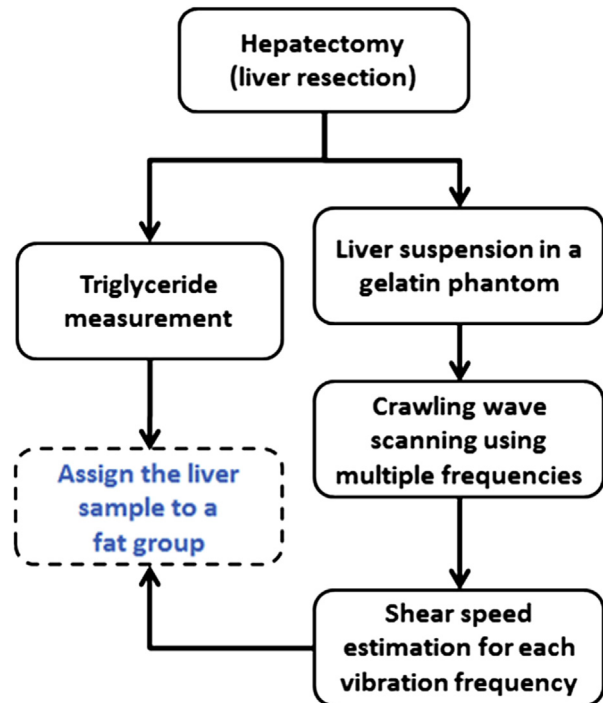


Fig. 4. Flowchart of the experimental procedure followed for each liver sample.

Separately, for crawling wave measurements, liver specimens were suspended in cubical molds using a 9.3% gelatin phantom. The phantom consisted of 2 L of degassed water, 409 g porcine gelatin (300 bloom pork gelatin, Gelatin Innovations, Schiller Park, IL, USA), 19.66 g salt (sodium chloride, BDH, West Chester, PA, USA) and 3.27 g agar (Difco Agar Technical Solidifying Agent, BD, Sparks, MD, USA). The components were mixed together and heated to 55°C. When it had been cooled to 32°C, the mixture was poured into the mold and placed in a refrigerator (approximately 5°C) for hardening. When solidified, the phantom was removed from the mold and allowed to rest at room temperature for about 7 h. CrW scanning was performed when the phantom reached room temperature, usually in the range 17°C to 19°C.

The CrW experimental setup is illustrated in Figure 1. The axes  $z$  and  $x$  correspond to the axial and lateral directions, respectively. A dual-channel function generator (Model AFG3022 B, Tektronix, Beaverton, OR, USA) was used to produce two sinusoidal signals with a slight difference of 0.6 Hz between the frequencies. The signals were passed through a power amplifier (Model 5530, AE Techron, Elkhart, IN, USA) and subsequently were supplied to piston vibration sources (Model 2706, Brüel and Kjaer, Naerum, Denmark). Two elongated bars with rough surfaces of  $8 \times 1 \text{ cm}^2$  were mounted on the pistons and placed in close contact at opposite sides of the phantom. The bars oscillated along a direction parallel to the sides of the phantom ( $z$ -axis), thereby generating shear wave propagation in the lateral direction ( $x$ -axis), from each side of the phantom. A linear array ultrasound transducer (L40-8/12 linear, Ultrasonix, Richmond, BC, Canada) was positioned between the vibration sources and scanned the medium.

A ROI within the liver specimen was chosen using the 15-MHz B-scan image of the liver for guidance. Then the color Doppler mode was turned on to scan the sample to produce a CrW movie. A single frame of the CrW movie is provided in Figure 5. Multiple frames (at least 100 frames; the maximum number of frames that can be saved depends on the color-flow ROI size) were acquired for each CrW movie by an ultrasound system (SonixTablet, Ultrasonix). The data were post-processed to generate a 3-D variance matrix, and subsequently the average shear speed was calculated using eqn (11). CrW experiments and subsequent shear speed estimations were performed for each liver sample using multiple discrete frequencies in the range [200, 360] Hz with frequency shifts of 0.6 Hz ( $f_1 = 200 \text{ Hz}$  and  $f_2 = 200.6 \text{ Hz}$ , and  $f_1 = 240 \text{ Hz}$  and  $f_2 = 240.6 \text{ Hz}$ , and so on). The CrW frequency range was appropriately chosen to increase the signal-to-noise ratio and reduce the reflections of the propagating shear waves at boundaries.

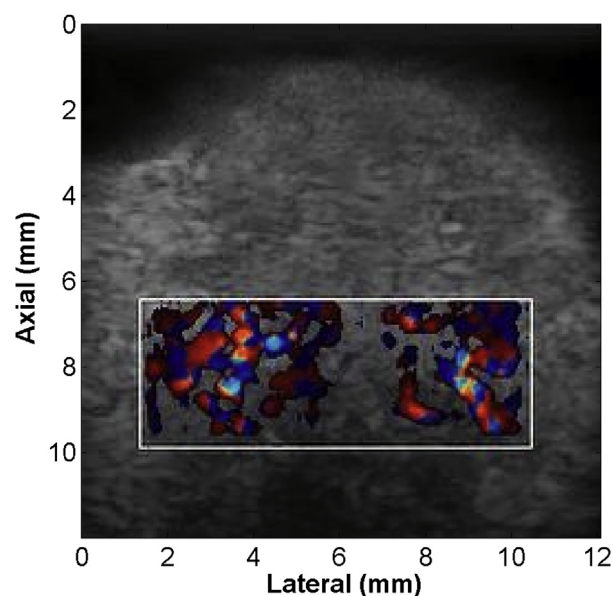


Fig. 5. B-Scan image of *ex vivo* mouse liver suspended in gelatin. Note region of interest with Doppler activation indicating crawling waves.

The raw data for each group consist of shear wave speed estimates at six discrete frequencies between 200 and 360 Hz. These data are fit to a linear regression to obtain the slope (dispersion in m/s per 100 Hz) and reference value at 250 Hz. The small size of each liver and limited frequency range studied make the dispersion (slope) calculation of each group more robust than use of the slopes of individual liver measurements.

On completion of the shear speed estimations and TG measurements for all liver samples, the data were organized with respect to the fat concentration for analysis as a group.

## RESULTS

The histogram distribution of the specimens with respect to TG concentration (mg/mg liver) is given in Figure 6. According to the histogram, it is natural to divide the livers into three groups. The average fat content in these three groups, as assessed by hematoxylin and eosin analysis of each specimen by our pathologist, was 19%, 53% and 78%. Dispersion analyses were performed within each group. All shear speed data are placed on the plot of shear speed versus frequency.

Figure 7(a–c) illustrates the shear speed estimates versus frequency and linear fits for the three groups (low, medium and high TG assays as denoted in Fig. 6). It can be seen that the slope, or dispersion, increases among the groups with higher triglyceride levels. However, the raw shear speeds in the range 200–250 Hz remain around 2.5 m/s in all three cases.

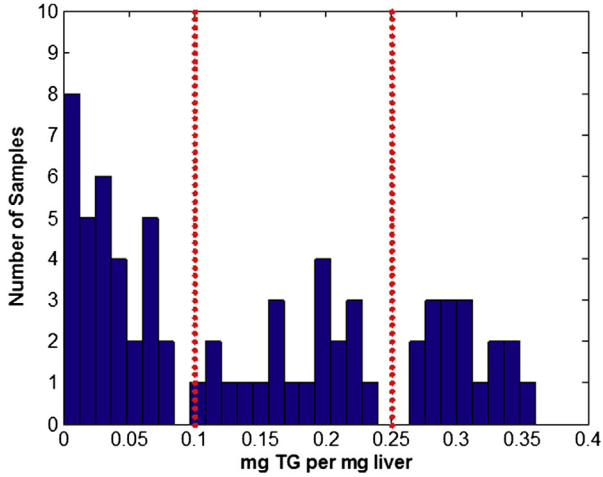


Fig. 6. Histogram of number of liver samples with respect to milligrams of triglyceride (TG) per milligram of liver. This histogram was generated on completion of the TG measurements for all liver samples. The livers were divided into three groups designated by the dotted lines.

The correlations,  $R^2$ , for the linear fits of these groups ranged between 0.84 and 0.92. The dispersion (slope) parameters (in cm/s/100 Hz of bandwidth) ranged from near 0 in the normal group to 0.347 in the high steatosis group. The dispersion (slope) of the high-steatosis group retains a value of 0.341 even when the three high outliers at high frequency in Figure 7c are removed from the group analysis.

Figure 8 provides a 2-D parameter space of dispersion (vertical axis) versus reference value of shear speed at 250 Hz (horizontal axis). The three boxes define the 90% confidence intervals for the linear fits of (slope, reference value) for the three groups in Figures 6 and 7. These boxes illustrate that dispersion slopes tend to increase with increasing triglyceride levels; however, the reference shear speed at 250 Hz is relatively unchanged.

### Statistical analysis

Paired series of scanning frequency (Freq) and shear speed ( $c_s$ ) were available for  $n = 68$  mice (2 of 70 were excluded for insufficient signal-to-noise), for each of which the TG/liver measurement was available. A group variable, Gr, was constructed by defining levels 1, 2 and 3 using respective rules TG/liver  $\in (0, 0.1)$ , TG/liver  $\in (0.1, 0.25)$  and TG/liver  $\in (0.25, 1)$ , according to the histogram in Figure 6. Plotting aggregate data for each individual mouse revealed a tendency toward more positive slopes for groups 2 and 3. In addition, the variance in  $c_s$  attributable to within-subject variation of Freq appears smaller than the variance in  $c_s$  across patients. For the subsequent analyses, we discarded a distinct subgroup of anomalous series within group 1, which is characterized by sharply

discontinuous values of  $c_s$  approaching  $\geq 3.5$  m/s at Freq values  $\geq 320$ . This rule was used to define anomalous patients, of which there were 7. No similar definition of anomaly was considered for the remaining groups. After removing anomalies, we had respective group sizes 25, 20 and 16 (=61). Although it is preferable that sample sizes are balanced by group, the correctness of the reported  $p$ -values and confidence intervals does not depend on this. All of the following statistical methods correctly account for the respective sample sizes, using standard methods. The linear regression fit  $c_s = \beta_0 + \beta_1(\text{Freq} - 360)$  was calculated, demonstrating a separation between group 1 and the remaining groups, but not between groups 2 and 3.

### Linear effects model

To more precisely quantify the  $c_s$  gradients, a linear mixed effects model was used. Within a single group, this is defineable as

$$c_{sij} = \beta_0 + B_{0i} + (\beta_1 + B_{1i})(\text{Freq}_{ij} - 360) + \varepsilon_{ij} \quad (12)$$

where  $i$  denotes the  $i$ th subject, and  $j$  identifies the  $j$ th data pair ( $\text{Freq}_{ij}, c_{sij}$ ) of subject  $i$ . For consistency, the model is similarly offset so that the intercept represents the fit at Freq = 360. The model is interpreted as follows: each subject  $i$  is assumed to have a distinct intercept  $\beta_0 + B_{0i}$  and slope  $\beta_1 + B_{1i}$ , where  $\beta_0$  and  $\beta_1$  are constant fixed effects, and the values of  $B_{0i}$  and slope  $B_{1i}$  are random effects assumed to be sampled from a normal distribution of mean 0. The model is therefore hierarchical in the sense that the slopes and intercepts for each subject are taken to be random samples from normal distributions of mean  $\beta_0$  and  $\beta_1$ . The fixed effects may be interpreted in the same way as for standard linear models, the role of the random effects being to model variation attributable to patients. The remaining term,  $\varepsilon_{ij}$ , then models variation not explained by the fixed and random effects combined, is assumed to be a random sample from a zero mean normal distribution and is independent of all other model elements. Group interactions may then be introduced in the standard manner as interaction terms, permitting the estimation of group effects for the slope and intercept.

Two models are considered, one using the three groups already defined and one in which groups 2 and 3 are pooled. The models (eqn [12]) were fit using the lme (linear mixed effects) function from the R statistical library (Pinheiro and Bates 2000). The fixed effects estimates are listed in Table 1. The  $p$ -value refers to the differences in  $\beta_0$  and  $\beta_1$  between group 1 and groups 2 and 3 in the first model and between group 1 and the pooled group for the second model (these differences are of more relevance than the absolute values). Examining both models, we can see that both  $\beta_0$  and  $\beta_1$  differ

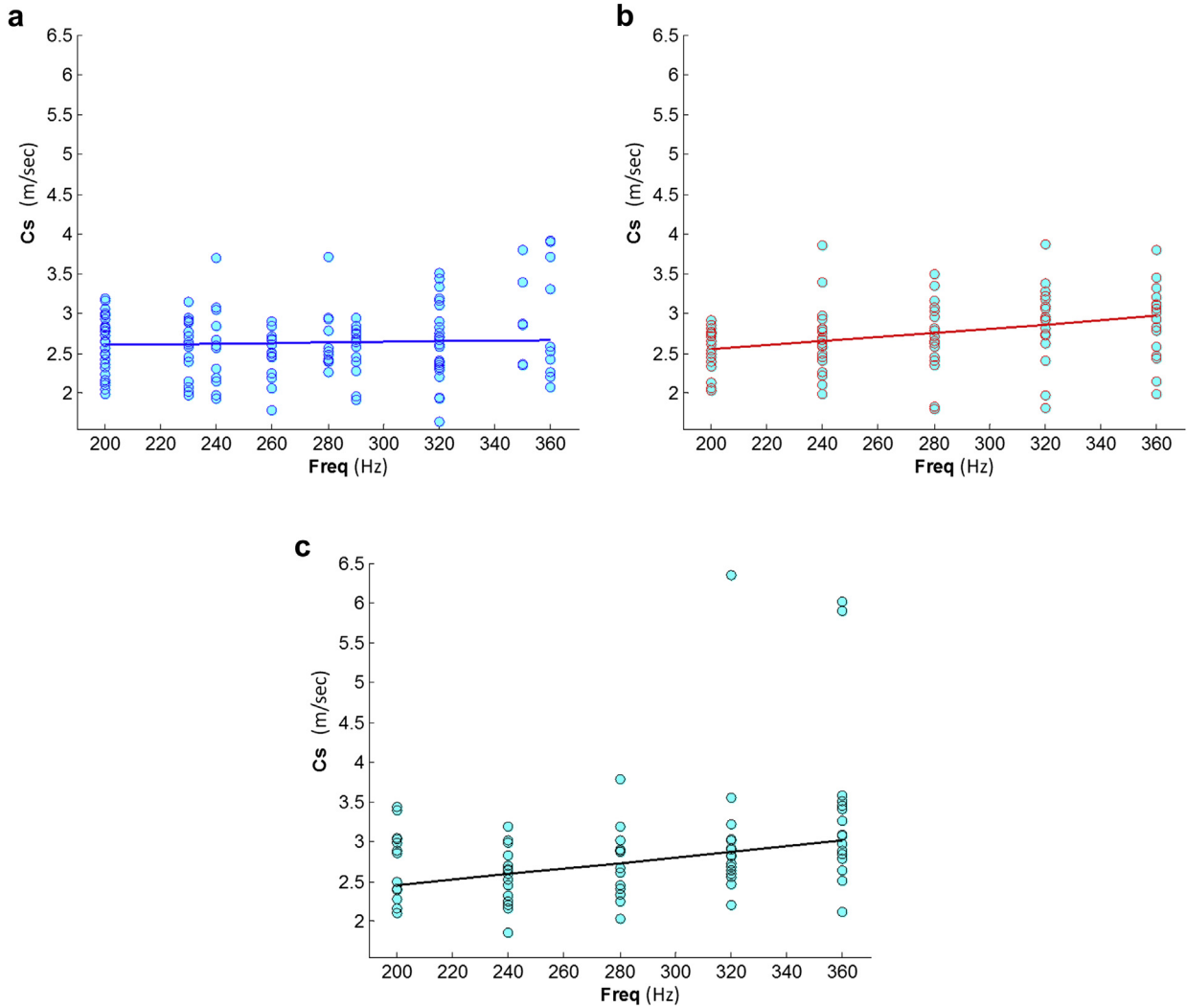


Fig. 7. Shear speed ( $c_s$ ) estimates versus frequency and linear fits for low (a), medium (b) and high (c) triglyceride assays as denoted in Figure 6. Vertical axis: shear speed in meters per second; horizontal axis: shear frequency in hertz.

significantly between group 1 and group 2 and between group 3 and groups 2 and 3 pooled. However, the parameters for groups 2 and 3 are approximately equal, the differences being within the respective standard errors. We therefore conclude that statistically significant differences in the  $c_s$ /Freq gradients and magnitudes exist between group 1 and the remaining groups, but also that groups 2 and 3 are not significantly different in this regard.

*Discriminant analysis*

We next consider the design of a classification rule. Following the previous analysis, groups 2 and 3 were pooled, and the classifier was based on the estimated values of  $\beta_0$  and  $\beta_1$ . Linear discriminant analysis (LDA) was used to estimate a linear classifier of the form  $\alpha_0\beta_0 + \alpha_1\beta_1$ . The coefficients  $\alpha_0 = 2.382$  and  $\alpha_1 = -14.79$  were obtained using the `lda` function

from the *R* statistical library (Venables and Ripley 2002), leading to classification score:

$$\text{score} = 2.382\beta_0 - 14.79\beta_1 \tag{13}$$

Figure 9 is a plot of the individually estimated values of the pairs  $(\beta_0, \beta_1)$ , with anomalies removed, and the group symbols indicate the two-group model. The dashed line illustrates the classification induced by setting score = 6.5, using eqn (13).

The LDA method may be used to estimate values of Freq at which observations of  $c_s$  have the greatest discriminating ability. We may express the linear discrimination function

$$\text{score} = \alpha_0\beta_0 + \alpha_1\beta_1 = c[\beta_0 + \beta_1(x - 360)] \tag{14}$$

so that in our model the score (eqn [13]) may be seen to be equivalent to selecting a value  $\text{Freq} = x$  at which a fitted

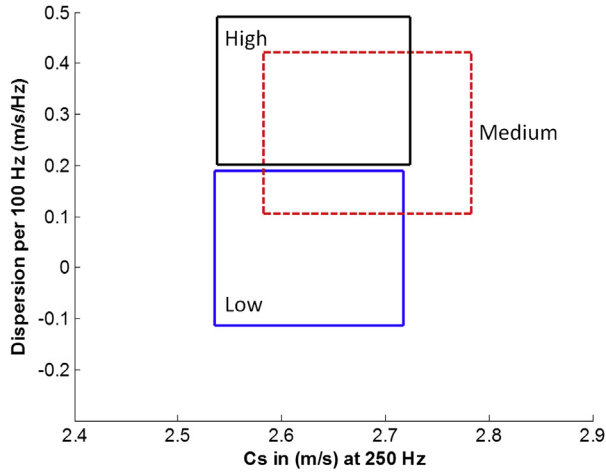


Fig. 8. Two-dimensional parameter space of dispersion (vertical axis) versus reference value of shear speed at 250 Hz (horizontal axis). The three boxes define the 90% confidence intervals for the linear fits (slope, reference value) for the three groups in Figures 6 and 7.

regression line has greatest discriminating ability. Given our values of  $\alpha_0$  and  $\alpha_1$ , eqn (14) may be solved to yield  $x = 353.8$ , from which we conclude that values of  $c_s$  observed near the upper limit of  $\text{Freq} = 360$  are to be preferred for classification.

In Figure 10(a) are receiver operating characteristic (ROC) curves, obtained by estimating true- and false-positive rates obtained by varying the *score* classification threshold. For the LDA regression method, rates were estimated using leave-one-out cross validation. The area under curve (AUC) statistic obtained was 83%, and estimates the probability that a pair of classification scores drawn randomly from each group are in the correct order. For comparison, the observed values of  $c_s$  at  $\text{Freq} = 280$  (the midpoint of the observed range) and  $\text{Freq} = 360$  were also used as classifiers, and the resulting ROC curves are also provided in Figure 10(b, c), with respective values of  $\text{AUC} = 72\%$  and  $\text{AUC} = 88\%$ . This supports the conclusion of the LDA analysis that values of  $c_s$  near  $\text{Freq} = 360$  have greater discriminating ability.

Table 1. Fixed effects for linear mixed effects models: three-group and two-group (pooled) models

Fit	Group	$\beta_0$	$p$ -value	$\beta_1$	$p$ -value
Three groups	TG/liver $\in (0, 0.1)$	2.35	—	-1.41 E-03	—
	TG/liver $\in (0.1, 0.25)$	2.92	0.0001	2.27 E-03	0.0004
	TG/liver $\in (0.25, 1)$	2.92	0.0001	2.07 E-03	0.0029
Two groups	TG/liver $\in (0, 0.1)$	2.35	—	-1.41 E-03	—
	TG/liver $\in (0.1, 1)$	2.92	0.0001	2.17 E-03	<0.0001

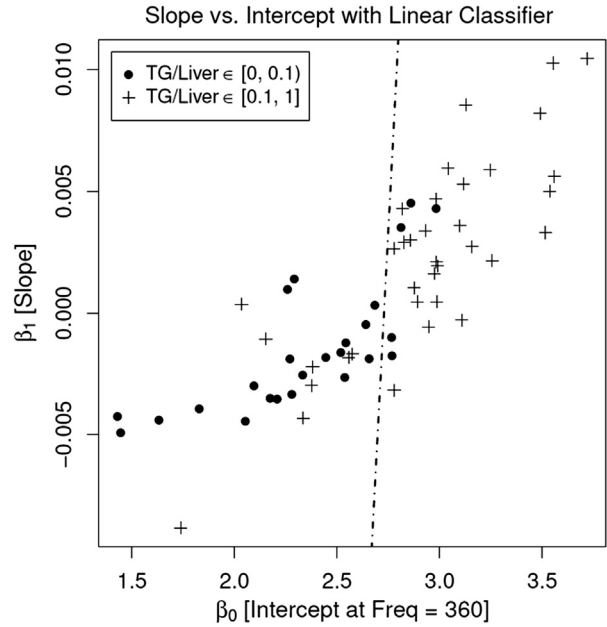


Fig. 9. Plot of pairs  $(\beta_0, \beta_1)$  for each mouse obtained by a linear regression fit of  $c_s$  against  $\text{Freq}$ , offset so that  $\beta_0$  represents the expected value of  $c_s$  at  $\text{Freq} = 360$  Hz. Anomalous pairs have been removed. Groups are distinguished by distinct symbols, as indicated in the legend (groups 2 and 3 are pooled). A classification induced by the linear classifier ( $\text{score} = 6.5$ ) is represented by the *dashed line*.

## DISCUSSION AND CONCLUSIONS

The dispersion within groups of livers is found to be near zero for normal livers (steatosis < 5%), increasing to 0.2–0.5 m/s per 100 Hz in the group with triglyceride levels >0.25 mg/mg liver. The possibility exists for staging progressive grades of steatosis by careful measurement of shear wave dispersion.

One limitation of our study was the difficulty in predicting steatosis accumulation simply based on the length of time mice were fed high-fat diets. Although we attempted to capture a range of steatotic livers by sampling at frequent time points, we encountered a rapid rise in steatosis over time and individual mouse variations in steatosis accumulation over time (data not shown). Future experiments should overcome these phenomena by increasing the number of animals studied and increasing the frequency of sampling, especially between weeks 6 and 16.

The lower range of clinically significant steatosis is generally regarded to be 30% of hepatocytes containing macrovesicular fat inclusions on hematoxylin and eosin staining of liver biopsy specimens. Above this range, patients are at higher risk of developing liver biochemical abnormalities and progression from simple steatosis to the fibro-inflammatory changes of non-alcoholic steatohepatitis (NASH). Also, the rates of primary liver

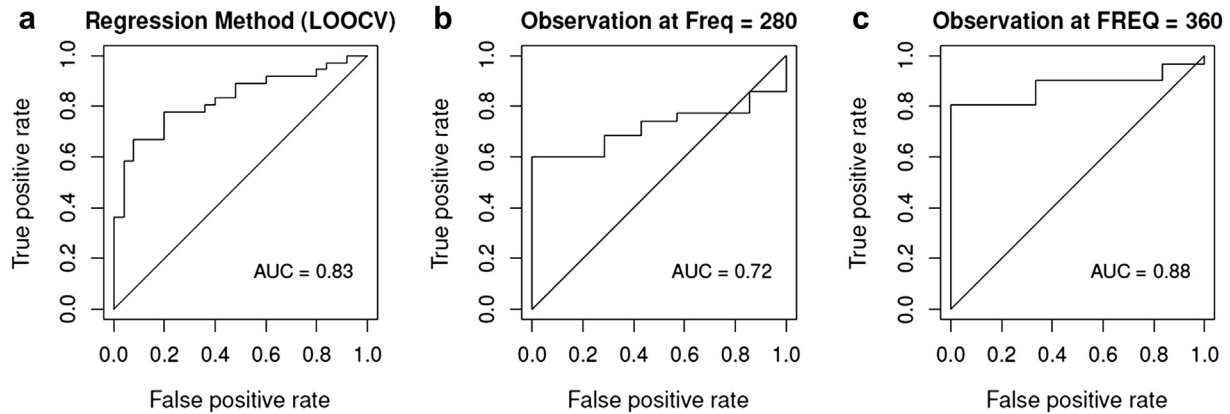


Fig. 10. (a) Receiver operating characteristic (ROC) curve for the linear discriminant analysis (LDA) classifier based on regression coefficients, with true- and false-positive rates estimated by leave-one-out cross validation (LOOCV). (b, c) ROC curves obtained by using  $c_s$  observations for Freq = 280 and Freq = 360, respectively. Anomalous pairs have been removed. In each plot the area under the curve (AUC) statistic is superimposed, and estimates the probability that a pair of classification scores drawn randomly from each group are in the correct order.

allograft dysfunction increase when organs with >30% macrosteatosis are transplanted. Our study found that low (<20%) and high (>50%) steatosis can be distinguished with crawling wave shear speed dispersion and that further study, including refinements in our technique and experimental design, is merited.

Other limitations of the study include the small sample volumes of mouse liver, the limited frequency range of the shear wave dispersion measurements and the use of *ex vivo* livers at room temperatures. *In vivo* liver values at body temperature will undoubtedly have different absolute values, and this may also alter the slope or dispersion dependence on the accumulation of fat. In addition, in some cases, shear wave reflections from adjacent boundaries (gel-liver) perturb the crawling wave patterns. These tend to be dependent on frequency, leading to higher variance in the resulting estimates of dispersion. This problem of proximal side boundaries is reduced in larger livers, and a modified configuration has been proposed to apply crawling waves through the abdominal wall in larger patients (Partin et al. *in press*). In this modified configuration, two shear wave sources are applied to the surface of the skin. The crawling wave pattern and estimates have been re-derived for this configuration, which is more suitable for *in vivo* human studies. Finally, in some humans, the additional presence of fibrosis, cirrhosis and inflammation will alter the baseline stiffness and shear speed, and it remains to be seen how the dispersion slope in these cases is altered by increasing grade of steatosis. We anticipate that optimization of a human scanning device will provide more accurate measurements of dispersion in individuals, because of increased ROI size and more distant reflecting boundaries. A group analysis based on a steatotic grading scale is likely to be useful as well.

Nonetheless, the results support the hypothesis that fat adds a viscous, lossy and therefore dispersive element to the liver, which can be estimated by measurement of dispersion.

**Acknowledgments**—This work was supported by the University of Rochester Department of Electrical & Computer Engineering and the University of Rochester Medical Center Departments of Surgery, Radiology, Biostatistics & Computational Biology and Pathology & Laboratory Medicine.

## REFERENCES

- Angulo P. Nonalcoholic fatty liver disease. *N Engl J Med* 2002;346:1221–1231.
- Barry CT, Mills B, Hah Z, Mooney RA, Ryan CK, Rubens DJ, Parker KJ. Shear wave dispersion measures liver steatosis. *Ultrasound Med Biol* 2012;38:175–182.
- Blackstock DT. *Fundamentals of physical acoustics*. New York: Wiley; 2000. ch 9.
- Burant CF, Sreenan S, Hirano KI, Tai TAC, Lohmiller J, Lukens J, Davidson NO, Ross S, Graves RA. Troglitazone action is independent of adipose tissue. *J Clin Invest* 1997;100:2900–2908.
- Castera L, Forns X, Alberti A. Non-invasive evaluation of liver fibrosis using transient elastography. *J Hepatol* 2008;48:835–847.
- Charlton M. Nonalcoholic fatty liver disease: A review of current understanding and future impact. *Clin Gastroenterol Hepatol* 2004;2:1048–1058.
- Chen J, Talwalkar JA, Yin M, Glaser KJ, Sanderson SO, Ehman RL. Early detection of nonalcoholic steatohepatitis in patients with nonalcoholic fatty liver disease by using MR elastography. *Radiology* 2011;259:749–756.
- Chen SG, Sanchez W, Callstrom MR, Gorman B, Lewis JT, Sanderson SO, Greenleaf JF, Xie H, Shi Y, Pashley M, Shamdasani V, Lachman M, Metz S. Assessment of liver viscoelasticity by using shear waves induced by ultrasound radiation force. *Radiology* 2013;266:964–970.
- De Ledinghen V, Vergniol J, Foucher J, Merrouche W, le Bail B. Non-invasive diagnosis of liver steatosis using controlled attenuation parameter (CAP) and transient elastography. *Liver Int* 2012;32:911–918.
- Dowman JK, Tomlinson JW, Newsome PN. Pathogenesis of non-alcoholic fatty liver disease. *QJM* 2010;103:71–83.
- Friedrich-Rust M, Muller C, Winckler A, Kriener S, Herrmann E, Holtmeier J, Poynard T, Vogl TJ, Zeuzem S, Hammerstingl R,

- Sarrazin C. Assessment of liver fibrosis and steatosis in PBC with FibroScan, MRI, MR-spectroscopy, and serum markers. *J Clin Gastroenterol* 2010;44:58–65.
- Friedrich-Rust M, Romen D, Vermehren J, Kriener S, Sadet D, Herrmann E, Zeuzem S, Bojunga J. Acoustic radiation force impulse-imaging and transient elastography for non-invasive assessment of liver fibrosis and steatosis in NAFLD. *Eur J Radiol* 2012;81: e325–e331.
- Hah Z, Hazard C, Mills B, Barry C, Rubens D, Parker K. Integration of crawling waves in an ultrasound imaging system: Part 2. Signal processing and applications. *Ultrasound Med Biol* 2012;38:312–323.
- Hazard C, Hah Z, Rubens D, Parker K. Integration of crawling waves in an ultrasound imaging system: Part 1. System and design considerations. *Ultrasound Med Biol* 2012;38:296–311.
- Hoyt K, Castaneda B, Parker KJ. Two-dimensional sonoelastographic shear velocity imaging. *Ultrasound Med Biol* 2008a;34:276–288.
- Hoyt K, Kneezel T, Castaneda B, Parker KJ. Quantitative sonoelastography for the in vivo assessment of skeletal muscle viscoelasticity. *Phys Med Biol* 2008b;53:4063–4080.
- Hoyt K, Parker KJ, Rubens DJ. Real-time shear velocity imaging using sonoelastographic techniques. *Ultrasound Med Biol* 2007;33: 1086–1097.
- Kasai C, Namekawa K, Koyano A, Omoto R. Real-time two-dimensional blood-flow imaging using an auto-correlation technique. *IEEE Trans Son Ultrason* 1985;32:458–464.
- Klain J, Fraser D, Goldstein J, Peiser J, Avinoah E, Ovnat A, Charuzi I. Liver histology abnormalities in the morbidly obese. *Hepatology* 1989;10:873–876.
- Levene AP, Kudo H, Armstrong MJ, Thursz MR, Gedroyc WM, Anstee QM, Goldin RD. Quantifying hepatic steatosis: More than meets the eye. *Histopathology* 2012;60:971–981.
- Marchesini G, Brizi M, Morselli-Labate AM, Bianchi G, Bugianesi E, McCullough AJ, Forlani G, Melchionda N. Association of nonalcoholic fatty liver disease with insulin resistance. *Am J Med* 1999;107: 450–455.
- Minervini MI, Ruppert K, Fontes P, Volpes R, Vizzini G, de Vera ME, Gruttadauria S, Miraglia R, Pipitone L, Marsh JW, Marcos A, Gridelli B, Demetris AJ. Liver biopsy findings from healthy potential living liver donors: Reasons for disqualification, silent diseases and correlation with liver injury tests. *J Hepatol* 2009;50:501–510.
- Partin A., Hah Z., Barry C.T., Rubens D.J. and Parker K.J., Elasticity estimates from images of crawling waves generated by miniature surface sources, *Ultrasound Med Biol*, DOI: 10.1016/j.ultrasmedbio.2013.05.019, in press [Epub ahead of print]
- Pinheiro JC, Bates DM. *Mixed-effects models in S and S-PLUS*. New York: Springer; 2000.
- Salameh N, Larrat B, Abarca-Quinones J, Pallu S, Dorvillius M, Leclercq I, Fink M, Sinkus R, Van Beers BE. Early detection of steatohepatitis in fatty rat liver by using MR elastography. *Radiology* 2009;253:90–97.
- Sasso M, Beaugrand M, de Ledinghen V, Douvin C, Marcellin P, Poupon R, Sandrin L, Miette V. Controlled attenuation parameter (CAP): A novel VCTE guided ultrasonic attenuation measurement for the evaluation of hepatic steatosis: Preliminary study and validation in a cohort of patients with chronic liver disease from various causes. *Ultrasound Med Biol* 2010;36:1825–1835.
- Sasso M, Tengher-Barna I, Zioli M, Miette V, Fournier C, Sandrin L, Poupon R, Cardoso AC, Marcellin P, Douvin C, de Ledinghen V, Trinchet JC, Beaugrand M. Novel controlled attenuation parameter for noninvasive assessment of steatosis using Fibroscan®: Validation in chronic hepatitis C. *J Viral Hepat* 2012;19:244–253.
- Schreuder TC, Verwer BJ, van Nieuwkerk CM, Mulder CJ. Nonalcoholic fatty liver disease: An overview of current insights in pathogenesis, diagnosis and treatment. *World J Gastroenterol* 2008;14: 2474–2486.
- Schwenzer NF, Springer F, Schraml C, Stefan N, Machann J, Schick F. Non-invasive assessment and quantification of liver steatosis by ultrasound, computed tomography and magnetic resonance. *J Hepatol* 2009;51:433–445.
- Selzner M, Clavien PA. Fatty liver in liver transplantation and surgery. *Semin Liver Dis* 2001;21:105–113.
- Strassburg CP, Manns MP. Approaches to liver biopsy techniques—Revisited. *Semin Liver Dis* 2006;26:318–327.
- Venables WN, Ripley BD. *Modern applied statistics with S*. New York: Springer; 2002.
- Wanless IR, Lentz JS. Fatty liver hepatitis (steatohepatitis) and obesity: An autopsy study with analysis of risk factors. *Hepatology* 1990;12: 1106–1110.
- Wu Z, Hoyt K, Rubens DJ, Parker KJ. Sonoelastographic imaging of interference patterns for estimation of shear velocity distribution in biomaterials. *J Acoust Soc Am* 2006;120:535–545.
- Wu Z, Taylor LS, Rubens DJ, Parker KJ. Sonoelastographic imaging of interference patterns for estimation of the shear velocity of homogeneous biomaterials. *Phys Med Biol* 2004;49:911–922.